Skillful spring forecasts of September Arctic sea ice extent using passive microwave sea ice observations

A. A. Petty[1,2], D. Schröder[3], J. C. Stroeve[4,5], T. Markus[2], J. Miller[2], N. T. Kurtz[2], D. L. Feltham[3], D. Flocco[3]

[1]Earth System Science Interdisciplinary Center, University of Maryland, College Park, MD, USA.

[2]Cryospheric Sciences Laboratory, NASA Goddard Space Flight Center, Greenbelt, MD, USA.

[3]Centre for Polar Observation and Modelling, Department of Meteorology, University of Reading, Reading, UK.

[4]National Snow and Ice Data Center, Cooperative Institute for Research in Environmental Sciences, University of Colorado, Boulder, Colorado, USA.

[5]Centre for Polar Observation and Modelling, University College London, London, UK.

Corresponding author: Alek A. Petty (alek.a.petty@nasa.gov)

Key Points:

- We demonstrate skillful spring forecasts of September Arctic sea ice extent using ice concentration and melt onset observations.
- Melt onset based forecast is the most skillful in early spring, while ice concentration forecast is more skillful from June onwards.
- Study provides insight into physical drivers of skillful seasonal forecasts including forecasts derived using simulated melt pond data.

Abstract

In this study we demonstrate skillful spring forecasts of detrended September Arctic sea ice extent using passive microwave observations of sea ice concentration (SIC) and melt onset (MO). We compare these to forecasts produced using data from a sophisticated melt pond model, and find similar to higher skill values, where the forecast skill is calculated relative to linear trend persistence. The MO forecasts shows the highest skill in March-May, while the SIC forecasts produce the highest skill in June-August, especially when the forecasts are evaluated over recent years (since 2008). The high MO forecast skill in early spring appears to be driven primarily by the presence and timing of open water anomalies, while the high SIC forecast skill appears to be driven by both open water and surface melt processes. Spatial maps of detrended anomalies highlight the drivers of the different forecasts, and enable us to understand regions of predictive importance. Correctly capturing sea ice state anomalies, along with changes in open water coverage appear to be key processes in skillfully forecasting summer Arctic sea ice.

1 Introduction

Arctic sea ice has decreased markedly over recent decades, and arguably the most recognizable indicator of this has been the rapid reduction in Arctic sea ice extent (SIE). Arctic SIE has declined across all seasons, with the strongest decline observed in September, the end of the summer melt season [e.g. *Serreze et al.*, 2007]. It is widely expected that Arctic SIE will continue to decline over the coming decades, resulting in a seasonally ice-free Arctic sometime this century [e.g. *Stroeve et al.,* 2012]. The role of internal variability in modulating the downward trend in SIE could be significant, and is still highly uncertain [e.g. *Swart et al.,* 2015, *Jahn et al*., 2016].

Increasing access to the Arctic marine environment has heightened the demand for more accurate seasonal sea ice forecasts [*Eicken*, 2013], and the rapid September SIE declines have prompted myriad investigations into summer sea ice predictability [e.g. *Guemas et al*., 2016, and references therein]. Previous studies have demonstrated strong correlation between spring Arctic sea ice-ocean conditions and September SIE, but no skill in seasonal forecasts (3 months or greater lead time) of de-trended SIE [e.g. *Lindsay et al*., 2008; *Blanchard-Wrigglesworth et al*., 2011]. Furthermore**,** a compilation of community sea ice forecasts produced by the Sea Ice Outlook (SIO) organized by the Study of Environmental Arctic Change (SEARCH) demonstrated that forecasts of summer SIE are unreliable [*Stroeve et al.*, 2014a], and are only slightly more skillful than assuming a simple linear trend. *Stroeve et al*., [2014a] also found that simple statistical forecasts often out-performed forecasts derived from more complex, dynamical sea ice models.

A recent study by *Schröder et al.* [2014], however, demonstrated skillful statistical forecasts of detrended September SIE based on spring melt pond coverage simulated using an explicit melt pond scheme [*Flocco et al.*, 2012] included in the sea ice model CICE (the forecast model is referred to as MP herein). The skill is thought to be due to a positive albedo feedback mechanism promoting sea ice loss: melt pond formation reduces the surface albedo, causing further absorption of solar radiation, and increased ice melt and melt pond formation [e.g. *Curry et al.,* 1995; *Perovich and Polashenski*, 2012].

The MP forecast utilizes a spatial correlation weighting prediction scheme first introduced for seasonal SIE predictions by *Drobot et al*. [2006] and adopted by *Lindsay et al*., [2008]. Briefly, grid cells of the chosen spring parameter (melt pond coverage in the MP model) are detrended and weighted based on their correlation with detrended September SIE. *Drobot et al*. [2006]

demonstrated an increase in predictive skill using weighted indices over simple pan-Arctic averages.

In this study we further explore the potential for skillful spring forecasts of September SIE using observations of spring sea ice conditions. We re-assess the potential for skillful SIE forecasts using passive microwave ice concentration data [*Cavalieri et al*., 1996, updated 2015], and also explore the use of spring melt onset data, derived from the same passive microwave sensor [*Markus et al*., 2009] as a further predictor of September SIE. Declines in sea ice have been linked with earlier sea ice melt onset [*Stroeve et al*., 2014b], and while the idea of melt onset as a summer sea ice predictor has been discussed in recent studies [e.g. *Kapsch et al*., 2014, *Mortin et al*., 2016], the data has yet to be fully assessed for its predictive capabilities. We also update the MP forecasts to 2016 and compare the skill of each forecast against linear trend persistence, arguably a fairer test of forecast skill than the detrended climatology often used in predictability studies [e.g. *Schröder et al*., 2014].

2 Data and methods

2.1 Sea ice data

In this study we utilize sea ice concentration (SIC) and melt onset (MO) data, both derived using passive microwave brightness temperature (T_b) estimates obtained from the Nimbus-7 Scanning Multichannel Microwave Radiometer (SMMR, 1978-1987), the Defense Meteorological Satellite Program (DMSP) F8, F11 and F13 Special Sensor Microwave/Imagers (SSM/Is, 1987-2008), and the DMSP F17 Special Sensor Microwave Imager/Sounder (SSMIS, 2009 to present). The F18 SSMIS sensor is also used for T_b estimates in May/June 2016, following the failure of DMSP F17. The SIC and MO data (1979-2015 climatology and 2016 raw/anomaly) are shown in

88 Figure 1.

89 Monthly SIC data from January 1979 to April 2015 are derived from T_b using the NASA Team
90 sea ice algorithm [*Cavalieri et al*., 1996, updated 2015]. Near-real time (NRT) daily
91 concentration data are available from May 2015 to the present day using the same NASA Team
92 processing of T_b [*Maslanik and Stroeve*, 1999, updated daily], from which monthly mean SICs
93 are computed. The data are provided on a 25 km x 25 km polar stereographic grid.

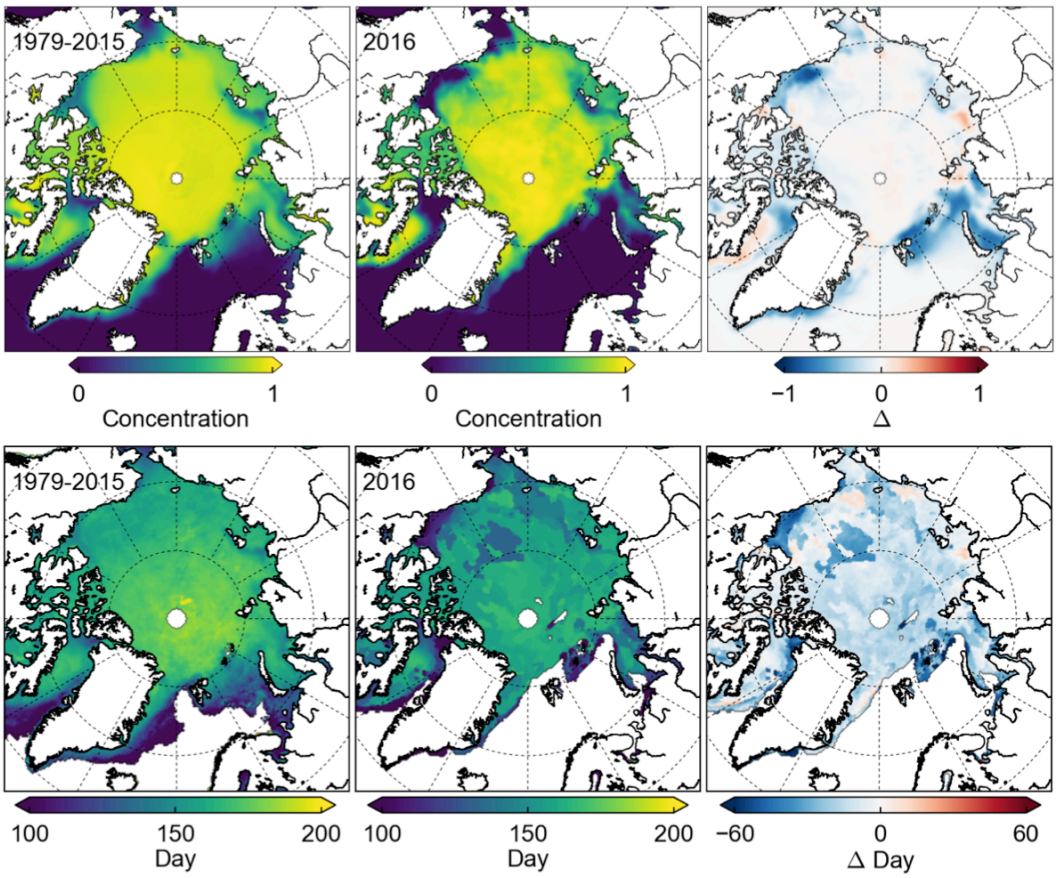

94

95 **Figure 1**: (top) June ice concentration using the NASA-Team algorithm for the 1979-2015
96 climatology (left), 2016 (middle), and the 2016 anomaly from climatology (right); (bottom) as in
97 (top) but for the day of continuous melt onset.

98 MO data from 1979 to 2016 (also on a 25 km x 25 km polar stereographic grid) are updated from
99 *Stroeve et al.,* [2014b] and *Markus et al.,* [2009]. MO estimates are based primarily on the

sensitivity of T_b to liquid water content in the overlying snow cover. The data give the day of the year for each grid-cell when continuous melt has begun (an early melt onset estimate is also produced). The full algorithm description is given in *Markus et al.,* [2009]. To include the changing areal coverage of open water in the MO data, all open water grid-cells are set to the minimum MO date (day 75). Another dataset is produced where the open water grid-cells are masked (MOmask). To produce forecasts using varying seasonal lead times, we express the MO data as the day before a given forecast date (e.g. the May forecast uses data up to day 151, the end of May). All melt onset days after this are then set to 0 (i.e. ice that has not melted). Note that both concentration and melt onset datasets contain the same time varying pole hole, depending on the passive microwave sensor used, which broadly translates to a pole hole north of 84.5 ^{o}N (1979-June 1987), 87.2 ^{o}N (July 1987– Dec 2007), 89.2 ^{o}N (2008 onwards).

We correlate the SIC and MO data with September Arctic SIE produced by the National Snow and Ice Data Center (NSIDC) Arctic Sea Ice Index, version 2 [*Fetterer et al*., 2016] using NASA Team ice concentration data.

2.2 Methods

We use the spatial detrending/weighting method utilized by *Schröder et al.,* [2014] and described in more detail by *Drobot et al.,* [2006, 2007] to include, and weight, only grid cells that correlate (historically) with September Arctic SIE. Note that a more detailed explanation of this forecast methodology is given in the supplementary information (Text S1). For each forecast, the gridded SIC/MO data from all years prior to the given forecast year are detrended (at least 3 years of data are needed to calculate a trend in each grid-cell). We calculate the Pearson product moment correlation coefficient (r) between the detrended SIC/MO data (of the given forecast month, for

each grid cell) and detrended September SIE (again only using data prior to the given forecast year). For the SIC (MO) data, negative (positive) r-values are set to 0. The method used here and in *Schröder et al.,* [2014] differs from *Drobot et al.,* [2006] in that only data preceding the given forecast year are included in the weighting calculation, and these weightings are thus updated each year.

The detrended gridded data from all years prior to the given forecast year are multiplied by the spatial weightings (r-values) and averaged across the pan-Arctic domain. A least-squares linear regression model is fit from this time series and the detrended SIE data. To produce a September SIE forecast, the SIC/MO data are detrended (spatially) using linear trend persistence, multiplied by the spatial weightings and averaged. This mean detrended/weighted forecast value is applied to the linear regression model to forecast the detrended September SIE anomaly. The forecast skill is given by

$$S = 1 - \sigma_{ferr}^2/\sigma_{anom}^2,$$

where σ_{anom} is the root mean squared error (RMSE) of the September SIE anomaly from linear trend persistence, and σ_{ferr} is the RMSE of the forecast. The forecast skill metric used in this study thus provides the skill of the forecast model relative to linear trend persistence. We initialize the forecasts in 1985. For SIC we use the mean, monthly SIC (focusing on May/June, but also provide forecast skill from earlier and later months). For MO, we use the MO date at the end of the relevant forecast month, and assume no information regarding MO past this date. We compare the SIC/MO forecasts with the updated May and June MP forecasts (up to 2016) and skill values calculated using the method described above. Note that the June MP forecast is produced using data integrated from the start of May to the end of June (June 25th). We also assess the potential improvement in forecast skill from the combination of these spring forecast

variables through multivariate linear regression, similar to the approach of *Lindsay et al.,* [2008].

3 Results and discussion

3.1 Assessing spring forecast skill

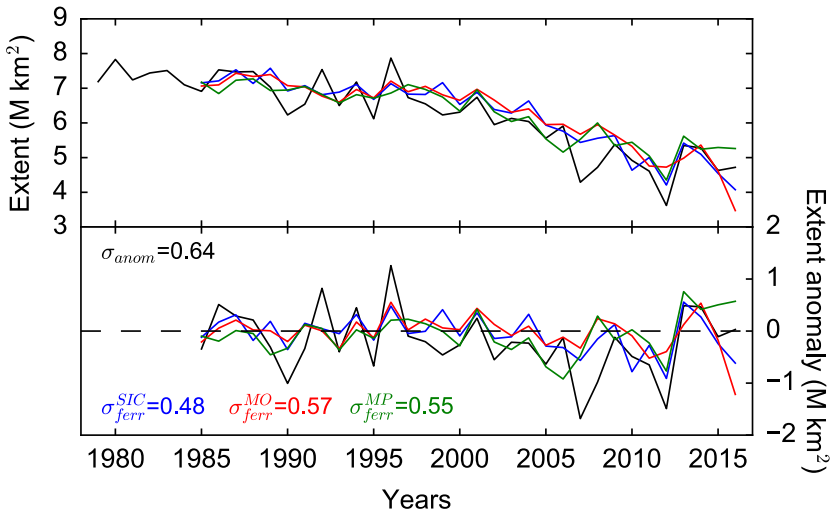

Figure 2: September sea ice extent (SIE) observed (black) and forecast using June sea ice concentration (SIC, blue), melt onset (MO, red, day 181) and melt pond (MP, green, May 1st-June 25th) forecast models. The SIE anomaly (bottom panel) is the anomaly compared to the SIE expected from linear trend persistence, σ_{anom} is the observed RMSE from linear trend persistence and σ_{ferr} is the RMSE for each forecast (1985-2016) in units of million km^2.

The June forecasts of September SIE using SIC, MO and MP data are shown in Fig. 2. Based on the RMSE of the detrended September SIE anomaly (from linear trend persistence), σ_{anom} = 0.64 million km^2, and the RMSE of the forecasts, σ_{ferr} = 0.48 (SIC), 0.57 (MO), 0.55 (MP) million km^2, the skill values for all three models are positive: S=0.44 (SIC), 0.20 (MO), 0.27 (MP), demonstrating clear seasonal forecast skill from all three models. The skill values from all three models at different forecast lead times are shown in Figure 3 (the importance of lead time is discussed later in the section). The May forecast skill values are lower than the June forecasts, but are still positive for all three models (the May forecasts are shown in Figure S1), with the MO model now slightly more skillful (S=0.19) than the SIC model (S=0.14) at this longer

forecast lead time. The skill values in May for SIC and MO are still higher than the MP skill (S=0.11). As noted by *Schröder et al.,* [2014], these positive skill values are remarkable when compared against the negative skill values of detrended SIE reported by *Lindsay et al.,* [2008].

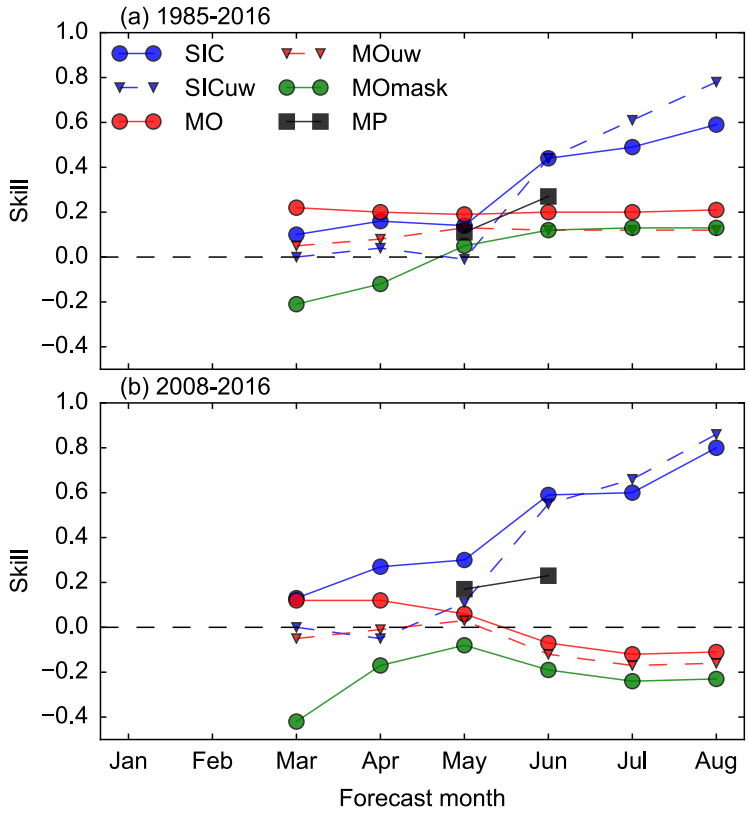

Figure 3: September Arctic sea ice extent forecast skill as a function of forecast month evaluated using (a) all years of forecasts (1985-2016), and (b) recent forecast years (2008-2016). Along with ice concentration (SIC), melt onset (MO) and melt pond (MP) forecast skill, the forecast skill is also shown for unweighted sea ice concentration (SICuw), unweighted melt onset (MOuw) and melt onset with open water masked (MOmask).

Figure 3 also shows the various forecast skills evaluated over the period 2008-2016, after the 2007 minimum and the start of the SEARCH SIO. For context, a simple estimate of the forecast skill based on the median June SIO forecasts of September SIE (2008-2016) results in a skill value of around zero (S=0.03). Compared to the longer evaluation period, the June skill values are higher for the SIC forecasts (S=0.59), but lower for the MP (S=0.23) and MO (S=-0.07). The

strong decline in the MO forecast skill is in part due to the 2016 forecast error (discussed later). Note also that σ_{anom} for this period is slightly higher at 0.65 million km^2.

To test whether the recent forecast skill is benefitting from the longer training time period from which the spatial trends and weightings are calculated, we also experimented with training the SIC forecast model with data from 2000 onwards (instead of 1979), and the June skill values (for forecasts since 2008) decreased (S=0.51 compared to 0.59), suggesting that higher skill in recent years is partially due to increased training of the forecast models. It is also thought that the strong interannual SIE variability experienced in the last several years means that linear trend persistence is less effective as a simple forecast estimate than it was in earlier decades, and the detrended anomalies are becoming more significant. This is expected from a thinner Arctic ice pack that is more responsive to atmospheric (and oceanic) forcing variability [e.g*., Holland et al.,* 2006].

3.2 Forecast skill as a function of lead time

To further understand the impact of lead time on the September SIE forecasts we produced multiple forecasts with lead times from March to August for both SIC and MO models, as shown in Figure 3 and summarized in Table 1. Analyzing first the 1985-2016 skill, the SIC forecasts show increasing skill from March (0.10) to August (0.59). The forecast skill increases significantly between May and June (0.14 to 0.44), showing that this transitionary period, where surface melt may be manifesting as concentration decreases, is an important time period for the SIC forecast model. The MO forecast skill is slightly higher than SIC in March to May (S=0.22-0.19), but does not show any significant increase with shorter lead times. In general, the results show that the MO model has higher forecast skill in March-May, but the SIC forecasts have the

best skill in June-August over this longer assessment period. The March MO skill (S=0.22) is perhaps the most skillful forecast of detrended September SIE currently available at this long (6 month) lead time. It appears that knowledge of when, not just where, regions became ice free is providing the high skill, as discussed more in the following section.

	SIC	MO	MP
March	0.10 / 0.13	0.22 / 0.12	-
April	0.16 / 0.27	0.20 / 0.12	-
May	0.14 / 0.30	0.19 / 0.06	0.11 / 0.17
June	0.45 / 0.60	0.21 / -0.04	0.27 / 0.23
July	0.49 / 0.60	0.20 / -0.12	-
August	0.59 / 0.80	0.21 / -0.11	-

Table 1: September Arctic sea ice extent forecast skill (S) as a function of forecast month (rows) using sea ice concentration (SIC), melt onset (MO) and melt pond (MP) data, evaluated over all forecast years (1985-2016, left) and recent forecast years (2008-2016, right).

For the 2008-2016 forecast skill (Figure 3b), SIC has the highest skill across all months (S=0.13 in March to 0.80 in August). The MO forecast skill is lower across all months, and even declines with lead time after May, suggesting MO is not as good a predictor of recent September SIE variability as it was in previous decades.

We also carried out multivariate regressions using combinations of the SIC, MO, and MP data (the skill values are shown in Figure S2). In general the multivariate regressions provided negligible, or even small declines in skill, except for the SIC/MP forecast, which showed a small increase in the 1985-2016 (June) and 2008-2016 (May and June) skill compared to the SIC forecast skill. The general lack of significant increase in skill across the multivariate regressions may be due to overfitting of these limited range datasets (also found and discussed in *Kapsch et al.,* [2014]), so more sophisticated methods of combining these datasets may be needed to increase overall skill, e.g. by accounting for open water/ice edge anomalies directly in the MP model.

3.3 Exploring the mechanisms promoting forecast skill

It is noteworthy that the forecast skill using simple observational sea ice state information, especially SIC, is higher than the MP forecast skill. Obviously one might also expect sea ice observations to provide more reliable information than a sea ice model, albeit a sophisticated one, as the results are not prone to errors in the model physics or inaccurate reanalyses. The SIC and MO forecasts utilize information regarding the changing coverage (and timing in the MO case) of open water, whereas the MP forecast only uses simulated surface melt pond information where there is ice each year. To explore this idea, we also carried out a forecast using the MO data, but where the open water grid-cells were masked (MOmask). This resulted in significantly lower skill values, including negative skill values before May (shown in Figure 3), implying that the inclusion of the variable open water coverage is driving the positive skill, and is thus a crucial process to capture for skillful spring forecasts, especially earlier in the year. The MO forecast provides added information over the SIC forecast as it says when (how long before the end of the given forecast month), not just where, grid cells became ice free. The increase in the MOmask skill from March-June implies that increased knowledge of the pan-Arctic MO is driving the increase in skill, however. The SIC forecast, however, includes the changing fraction of open water, not just whether a grid-cell is ice free. The high skill in the SIC forecasts is also likely driven by the inclusion of surface melt in the SIC data, and the implicit detection of melt ponds (May onwards), which can be interpreted as open water by the passive microwave sensor [e.g. *Kern et al*., 2016]. The SIC forecast therefore likely incorporates elements of the surface melt feedback described earlier with respect to the MP forecast. Consequently, it is perhaps unsurprising that SIC would provide the most skillful forecasts, especially at shorter lead times.

The skill in both MO and SIC forecasts thus appears to be driven, in-part, by capturing the

location of the spring ice edge and an open water positive feedback loop within the ice pack (in the SIC forecast): increased open water due to sea ice loss reduces the surface albedo, causing further absorption of solar radiation and sea surface temperature increases, driving increased open water [e.g. *Perovich et al*., 2007]. The timing of ice retreat will determine how long the open water has been exposed to solar heat absorption, giving rise to warmer sea surface temperatures [*Steele and Dickinson*, 2016] and additional sea ice melt. This is thought to be the dominant mechanism driving the high skill in the MO forecast, especially in early spring, as the timing of ice retreat is well correlated with the timing of MO [*Stroeve et al*., 2016]. The SIC model, however, is benefitting from combined knowledge of open water and an additional surface melt/melt pond feedback mechanism, especially later in spring. Note that to impact the summer ice pack, these spring open water/surface temperature anomalies must have non-local effects through, e.g. a northward advection of surface temperature anomalies (from the increased solar radiation absorption) increasing basal/lateral ice melt, or changing ice drift patterns (a weakening of the ice pack and increased ice drift into regions of higher melt potential).

3.4 The physical drivers of high forecast skill

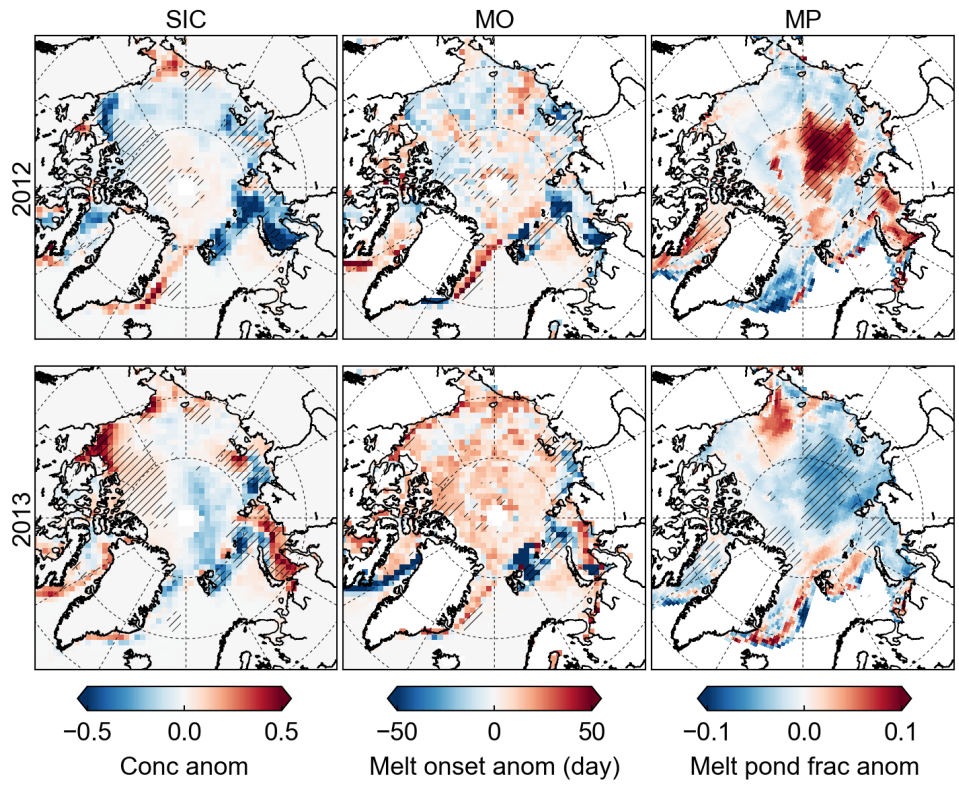

Figure 4. Detrended anomalies (anom) of sea ice concentration (SIC), melt onset (MO) and melt pond fraction (MP) data in June, used to drive the 2012/2013 forecasts. Note that a negative melt onset anomaly signifies melting earlier in the year. The hatchings indicate regions where the correlation coefficient (r) between the detrended springtime forecast variable and September sea ice extent (spatial weightings) for all years prior to the forecast year is greater than 0.3.

Figure 4 shows the detrended anomalies and spatial weightings used to generate the June forecasts in 2012 (2013), an anomalously low (high) September SIE year. Figure 4 clearly shows negative SIC anomalies in the Barents, Kara and southeastern Beaufort seas in 2012, but positive anomalies in the southeastern Beaufort and Kara Sea in 2013. The spatial weightings (hatched regions in Figure 4) show more extensive regions of historical correlation with September SIE (prior to 2012/2013) for the SIC than for the MO forecasts, which may also be contributing to the increased skill (i.e. there is more data being used to drive the SIC forecasts). Note that complete spatial weighting maps are shown in Figure 5 (using all data up to 2015) highlighting the variability in weightings across the three forecasts. Figure 5 also shows how the regions of high

correlation increase from the May to June forecasts in the SIC and MP forecasts, but not in the MO forecast. The large region of high ($r > 0.3$) spatial weighting north of the Beaufort Sea and the Canadian Archipelago in the SIC model appears after 2007, when strong spring SIC declines in the region coincided with the record low September SIE that year. It is interesting to note that the spatial weightings and anomalies in the MP forecast are located predominantly within the Central Arctic region (in both 2012 and 2013). In contrast, the SIC and MO forecast models show stronger weightings/anomalies in the peripheral seas: the result of anomalies around the spring sea ice edge.

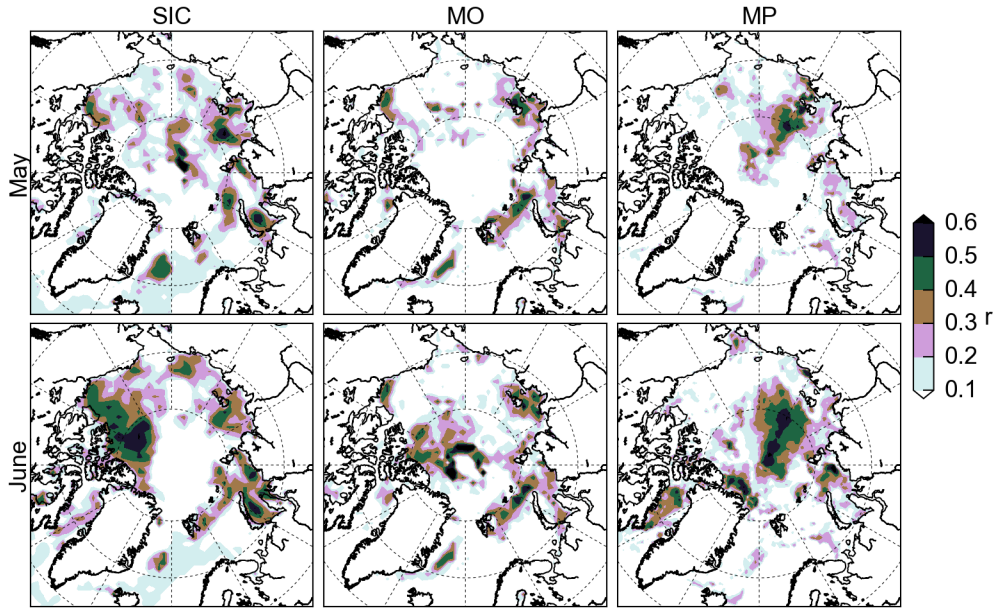

Figure 5. Spatial weightings used in the 2016 May (top row) and June (bottom row) sea ice concentration (SIC), melt onset (MO), and melt pond (MP) forecasts. The weighting indicates the correlation coefficient (r) between the springtime forecast variable and September sea ice extent.

To test the impact of the spatial weighting scheme on the forecast skill, we also produced forecasts where the detrended SIC/MO forecast data were not weighted based on past correlation with September SIE (SICuw and MOuw). The spatial weightings provide an increase in skill for all months of the MO forecasts and for the March-May SIC forecasts, but interestingly, for the

July/August SIC forecasts, the unweighted method's skill is higher (for both the 1985-2016 and 2008-2016 skill, as shown in Figure 3). While this was somewhat surprising, it does make physical sense. The spatial weightings are needed earlier in spring to remove grid cells from the averaging process that have experienced anomalies that are unimportant for September SIE, e.g. regions unlikely to melt out by the end of summer. However, in late spring/early summer, SIC anomalies are more likely to have a significant impact on the end of summer sea ice state even if these anomalies occur in regions that have not experienced sea ice anomalies before, or that are historically uncorrelated with September SIE. Including these new regions may allow us to better capture unprecedented extremes in September SIE. This raises a general difficulty facing sea ice forecasting: coping with the rapid declines in Arctic sea ice and the lack of historical equivalence to the anomalous behavior exhibited in recent years.

3.4 Remarks on the 2016 forecasts

2016 has been an exceptional year in the Arctic, with record high surface temperatures [e.g. *Cullather et al*. 2016] and record low Arctic SIE observed throughout much of winter and spring [e.g. http://www.ncdc.noaa.gov/sotc/summary-info/global/201606]. While in recent years the three individual forecast models (SIC/MO/MP) all seem to broadly agree on the expected interannual variability in September SIE e.g. the anomalously low (high) SIE in 2012 (2013), the models offered contrasting forecasts for 2016. Using data up to June 2016, the SIC and MO models forecast an anomalously low (potentially record low) September SIE of 3.5 M km^2 (MO) and 4.1 M km^2 (SIC), which are below that expected from linear trend persistence. Figure 6 shows the detrended anomalies and spatial weightings used to generate the 2016 (and 2015) forecasts, with the spatial patterns of SIC and MO anomalies similar to 2012; low SIC and early melt onset/ice retreat (earlier than any other year in the satellite record) suggesting low SIE. The

MP model, however, forecast (in June) a September SIE of 5.2 M km^2, similar to the 2015 MP forecast, and above that expected from linear trend persistence. A relatively cold and cloudy June appeared to hinder the formation of melt ponds, suggesting a higher September SIE than the SIC and MO model. Note that the SIC and MP May/June forecasts were submitted to the SEARCH SIO.

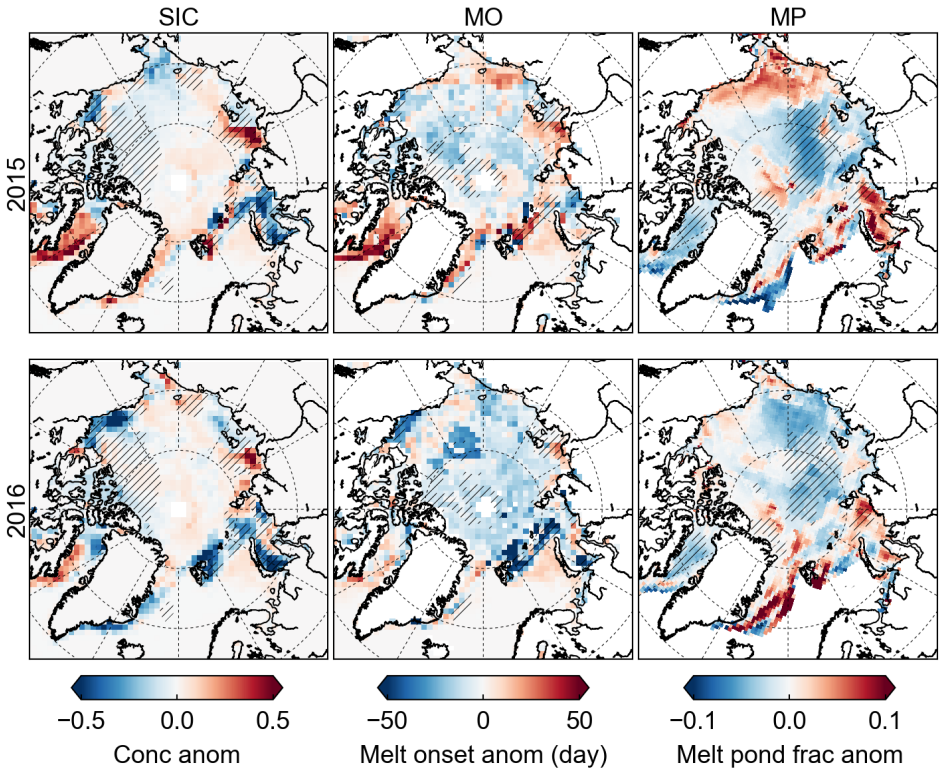

Figure 6: As in Figure 4, but for the data used to drive the 2015/2016 forecasts.

The observed September SIE was recently reported by the NSIDC as 4.72 M km^2, slightly above that expected from linear trend persistence and in-between the three June forecasts. Note that the May MP forecast of 4.5 M km^2 was, in fact, closer to the observed value than any of the spring forecasts presented in this study, while the July SIC forecast was 4.4 M km^2, showing reasonable convergence towards the observed SIE. The September Arctic sea ice pack was observed to be low in concentration over a large swath of the Central Arctic following two cyclones that entered

the Arctic in August (https://nsidc.org/arcticseaicenews/2016/09/arctic-sea-ice-nears-its-minimum-extent-for-the-year/). This ice pack will have the same SIE as a more consolidated ice pack spanning the same total area, highlighting a general difficulty with forecasting SIE. Forecasts arguably should not be judged based on one year alone, but 2016 clearly highlights that we are still unable to produce consistently accurate September Arctic SIE forecasts despite our high forecast skill.

3.5 Towards regional forecasting

An Alaskan SIE was also solicited from the SIO in 2016 (covering the Beaufort/Chukchi/Bering seas defined by the NSIDC region mask used in *Stroeve et al.,* [2014b] and shown in Figure S3). To briefly explore the ability of our approach for producing skillful regional forecasts we trained and forecast September Alaskan SIE using the SIC data. The forecast model (using June SIC data) is shown in Figure 7. The Alaskan SIE forecast skill is high for both 1985-2016 (S=0.40) and 2008-2016 (S=0.78) assessment periods, while the 2016 forecast of Alaskan SIE (0.30 M km^2) was the closest to the observed value (0.27 M km^2) of the four forecasts submitted to the SIO. While regional forecasting was not a primary focus of this paper, the skillful Alaskan SIE forecast is promising and suggests more localized forecasts could be provided based on stakeholder needs.

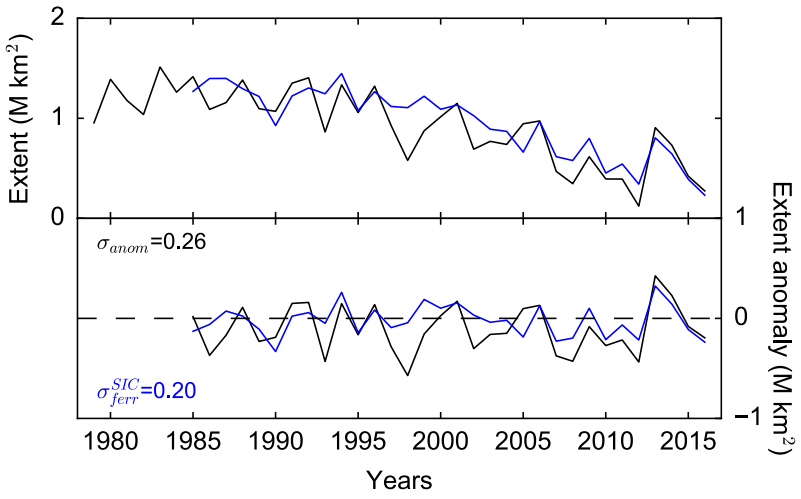

Figure 7: Alaskan September sea ice extent (SIE) observed (black) and forecast using June sea ice concentration (SIC, blue). The SIE anomaly (bottom panel) is the anomaly compared to the SIE expected from linear trend persistence, σ_{anom} is the observed RMSE from linear trend persistence, and σ_{ferr} is the RMSE of the forecast (1985-2016) in units of million km^2.

4 Conclusions

It is clearly impossible to perfectly forecast September SIE in spring, due to the impact of unknown summer weather conditions that impact sea ice variability through thermodynamic and dynamic processes [e.g. *Serreze et al*., 2016]. In this study, however, we have demonstrated skillful spring forecasts of detrended September sea ice extent (SIE) using passive microwave observations of sea ice concentration (SIC) and melt onset (MO) within a simple linear regression model framework. These forecast skill values are similar or higher than the skill values found using melt pond data simulated by a sophisticated melt pond model. The MO forecast shows higher skill in the March-May forecasts (compared to the SIC and MP models), with the positive forecast skill in March perhaps the highest forecast skill of detrended September SIE found at this lead time. The SIC model shows the highest skill in the June-August forecasts, especially when assessed over recent years (since 2008). The SIC data is available near-real time and may have been overlooked as a source of skillful seasonal sea ice forecasts.

The spatial maps of detrended anomalies provide a useful means of understanding the drivers of springtime forecasts of September SIE, and enable us to highlight regions of predictive importance – e.g. the Beaufort, Barents and Kara seas. Spatially weighting the data for forecasts made before June provides a significant increase in skill (through including only regions of historical correlation with September sea ice), while our results also suggest using unweighted spatial data can improve the skill of forecasts made after June (capturing unprecedented anomalies). While the melt pond forecast skill appears to be driven by a surface albedo feedback mechanism, the ice concentration and melt onset forecast skill appear to benefit from incorporating changes in the location of the spring ice edge and an additional open water positive feedback loop within the ice pack (in the SIC forecast), especially later in spring. Correctly capturing sea ice state anomalies, along with changes in the ice edge location/coverage thus appear key to increasing seasonal summer sea ice forecast skill (e.g. the open water information missing from the melt pond forecast model).

Acknowledgments and Data

The ice concentration data are made available through the NSIDC (http://nsidc.org/data/nsidc-0051 and https://nsidc.org/data/nsidc-0081), while the melt onset data are available at NASA's Cryospheric Sciences homepage (http://neptune.gsfc.nasa.gov/csb/index.php?section=54). All other data and processing scripts used to drive the various forecasts have been made publically available at http://www.github.com/akpetty/ArcticSeaIcePrediction2017.git. The primary author can be contacted for any further data requests.

We thank the reviewers and editor for their assistance in evaluating the manuscript, and would also like to the NASA Goddard Space Flight Center, Cryospheric Sciences sea ice group for

inspiring conversations regarding the data and methods used in this study.

References

Blanchard-Wrigglesworth, E., K. C. Armour, C. M. Bitz, and E. DeWeaver (2011), Persistence and Inherent Predictability of Arctic Sea Ice in a GCM Ensemble and Observations, *J. Climate*, *24*(1), 231–250, doi:10.1175/2010JCLI3775.1.

Cavalieri, D., Parkinson, Claire, Gloersen, Per, and Zwally, Jay. H (1996), Sea Ice Concentrations from Nimbus-7 SMMR and DMSP SSM/I-SSMIS Passive Microwave Data, Version 1, Boulder, Colorado USA: NASA DAAC at the National Snow and Ice Data Center, doi:10.5067/8GQ8LZQVL0VL.

Cullather, R. I., Y.-K. Lim, L. N. Boisvert, L. Brucker, J. N. Lee, and S. M. J. Nowicki (2016), Analysis of the warmest Arctic winter, 2015–2016,Geophys. Res. Lett., 43, doi:10.1002/2016GL071228.

Curry, J. A., J. L. Schramm, and E. E. Ebert (1995), Sea Ice–Albedo Climate Feedback Mechanism, *J. Climate*, *8*(2), 240–247, doi:10.1175/1520-0442(1995)008<0240:SIACFM>2.0.CO;2.

Drobot, S. D. (2007), Using remote sensing data to develop seasonal outlooks for Arctic regional sea-ice minimum extent, *Remote Sensing of Environment*, *111*(2–3), 136–147, doi:10.1016/j.rse.2007.03.024.

Drobot, S. D., J. A. Maslanik, and C. Fowler (2006), A long-range forecast of Arctic summer sea-ice minimum extent, *Geophys. Res. Lett.*, *33*(10), L10501, doi:10.1029/2006GL026216.

404 Eicken, H. (2013), Ocean science: Arctic sea ice needs better forecasts, *Nature*, *497*(7450), 431–
405 433, doi:10.1038/497431a.

406 Fetterer, F., K. Knowles, W. Meier, and M. Savoie. 2016, updated daily. *Sea Ice Index, Version*
407 *2*. Boulder, Colorado USA. NSIDC: National Snow and Ice Data Center.
408 doi:http://dx.doi.org/10.7265/N5736NV7.

409 Flocco, D., D. Schröder, D. L. Feltham, and E. C. Hunke (2012), Impact of melt ponds on Arctic
410 sea ice simulations from 1990 to 2007, *J. Geophys. Res.*, *117*,
411 doi:10.1029/2012JC008195.

412 Guemas, V. et al. (2016), A review on Arctic sea-ice predictability and prediction on seasonal to
413 decadal time-scales, *Q.J.R. Meteorol. Soc.*, *142*(695), 546–561, doi:10.1002/qj.2401.

414 Holland, M. M., C. M. Bitz, and B. Tremblay (2006), Future abrupt reductions in the summer
415 Arctic sea ice, Geophys. Res. Lett., 33, L23503, doi:10.1029/2006GL028024.

416 Jahn, A., J. E. Kay, M. M. Holland, and D. M. Hall (2016), How predictable is the timing of a
417 summer ice-free Arctic?, Geophys. Res. Lett., 43, 9113–9120,
418 doi:10.1002/2016GL070067.

419 Kapsch, M.-L., R. G. Graversen, T. Economou, and M. Tjernström (2014), The importance of
420 spring atmospheric conditions for predictions of the Arctic summer sea ice extent,
421 *Geophys. Res. Lett.*, *41*(14), 5288–5296, doi:10.1002/2014GL060826.

422 Kern, S., A. Rösel, L. T. Pedersen, N. Ivanova, R. Saldo, and R. T. Tonboe (2016), The impact
423 of melt ponds on summertime microwave brightness temperatures and sea-ice
424 concentrations, *The Cryosphere*, *10*(5), 2217–2239, doi:10.5194/tc-10-2217-2016.

425 Lindsay, R. W., J. Zhang, A. J. Schweiger, and M. A. Steele (2008), Seasonal predictions of ice

426 extent in the Arctic Ocean, *J. Geophys. Res.*, *113*(C2), doi:10.1029/2007JC004259.

427 Markus, T., J. C. Stroeve, and J. Miller (2009), Recent changes in Arctic sea ice melt onset,
428 freezeup, and melt season length, *J. Geophys. Res.*, *114*, doi:10.1029/2009JC005436.

429 Maslanik, J., and J. C. Stroeve (1999), Near-Real-Time DMSP SSMIS Daily Polar Gridded Sea
430 Ice Concentrations, Version 1. [December 2015-January 2016]. Boulder, Colorado USA:
431 NASA DAAC the National Snow and Ice Data Center, doi:10.5067/U8C09DWVX9LM.

432 Mortin, J., G. Svensson, R. G. Graversen, M.-L. Kapsch, J. C. Stroeve, and L. N. Boisvert
433 (2016), Melt onset over Arctic sea ice controlled by atmospheric moisture transport,
434 *Geophys. Res. Lett.*, doi:10.1002/2016GL069330.

435 Perovich, D. K., and C. Polashenski (2012), Albedo evolution of seasonal Arctic sea ice,
436 *Geophys. Res. Lett.*, *39*, doi:10.1029/2012GL051432.

437 Perovich, D. K., B. Light, H. Eicken, K. F. Jones, K. Runciman, and S. V. Nghiem (2007),
438 Increasing solar heating of the Arctic Ocean and adjacent seas, 1979–2005: Attribution
439 and role in the ice-albedo feedback, *Geophys. Res. Lett.*, *34*(19),
440 doi:10.1029/2007GL031480.

441 Schröder, D., D. L. Feltham, D. Flocco, and M. Tsamados (2014), September Arctic sea-ice
442 minimum predicted by spring melt-pond fraction, *Nature Clim. Change*, *4*(5), 353–357,
443 doi:10.1038/nclimate2203.

444 Serreze, M. C., M. M. Holland, and J. Stroeve (2007), Perspectives on the Arctic's Shrinking
445 Sea-Ice Cover, *Science*, *315*(5818), 1533–1536, doi:10.1126/science.1139426.

446 Serreze, M. C., J. Stroeve, A. P. Barrett, and L. N. Boisvert (2016), Summer atmospheric
447 circulation anomalies over the Arctic Ocean and their influences on September sea ice

448 extent: A cautionary tale, *J. Geophys. Res. Atmos.*, 2016JD025161,
449 doi:10.1002/2016JD025161.

450 Steele, M., and S. Dickinson (2016), The phenology of Arctic Ocean surface warming, *J.*
451 *Geophys. Res. Oceans*, 121, doi:10.1002/2016JC012089.

452 Stroeve, J. C., V. Kattsov, A. Barrett, M. Serreze, T. Pavlova, M. Holland, and W. N. Meier
453 (2012), Trends in Arctic sea ice extent from CMIP5, CMIP3 and observations, *Geophys.*
454 *Res. Lett.*, *39*(16), doi:10.1029/2012GL052676.

455 Stroeve, J., L. C. Hamilton, C. M. Bitz, and E. Blanchard-Wrigglesworth (2014a), Predicting
456 September sea ice: Ensemble skill of the SEARCH Sea Ice Outlook 2008–2013,
457 *Geophys. Res. Lett.*, *41*(7), 2411–2418, doi:10.1002/2014GL059388.

458 Stroeve, J. C., T. Markus, L. Boisvert, J. Miller, and A. Barrett (2014b), Changes in Arctic melt
459 season and implications for sea ice loss, *Geophys. Res. Lett.*, *41*(4), 1216–1225,
460 doi:10.1002/2013GL058951.

461 Stroeve, J. C., A. D. Crawford, and S. Stammerjohn (2016), Using timing of ice retreat to predict
462 timing of fall freeze-up in the Arctic, *Geophys. Res. Lett.*, doi:10.1002/2016GL069314.

463 Swart, N. C., J. C. Fyfe, E. Hawkins, J. E. Kay, and A. Jahn (2015), Influence of internal
464 variability on Arctic sea-ice trends, *Nature Clim. Change*, *5*(2), 86–89,
465 doi:10.1038/nclimate2483.